Optimization of Transfer Times in Pinned Photodiodes

Lutz Girgenrath[1,3], Martin Hofmann[1], Ralf Kühnhold[1] and Holger Vogt[2,3]
[1] *ELMOS Semiconductor AG, Heinrich-Hertz-Str. 1, 44227 Dortmund, Germany*
[2] *Fraunhofer Institute for Microelectronic Circuits and Systems, Finkenstrasse 61, 47057 Duisburg, Germany*
[3] *University Duisburg-Essen, Duisburg, Germany*

Keywords: CMOS Imaging, Lateral Drift-field Photodetectors (LDPD), High-speed Imaging, Large Pixels.

Abstract: An implantation scheme which enhances the readout speed of a silicon pinned photodiode (PPD) with large pixel length is presented. The basic PPD structure was developed for Time-of-Flight (TOF) distance measurement applications by the Fraunhofer IMS in Duisburg, Germany, and was fabricated in a standard 0.35 μm CMOS process. The optimized design of this PPD introduces the possibility to improve the electron readout speed by changing the n-well configuration with a second well implantation. The local increase in doping concentration creates a designated electron path which utilizes the reset voltage of the readout node. This behaviour is shown by simulation and measurement results are presented.

1 INTRODUCTION

In recent years, the usage of optical and contactless distance measurements like phase-modulation or time-of-flight has increased. These types of measurements require high speed and high performance sensors which are already widely used in entertainment systems. In the last years they found their way into the automotive sector for distance measurements and gesture control. Since these systems require information about the light pulse or phase, an external light source is needed to illuminate the area. The usage of IR-light is mandatory for scanning applications in terms of eye safety and distraction. However, the quantum efficiency (QE) of silicon for this part of the spectrum is rather poor ((Green and Keevers, 1995)) and the sensors reach their limits when an application needs both a high sensitivity and a fast signal acquisition. Since the sensitivity is defined mainly by the photosensitive area, one must use large diodes especially when operated in unfavourable environments or with IR-light. However, increasing the sensor area leads to a longer transfer time due to the quadratic dependence between the length of the electron path and the transfer time. Many groups tried to mitigate this behaviour for smaller PPD ((Xu and Theuwissen, 2013), (Tubert et al., 2009), (Han, 2015)). The goal of this work is to maximize the diode length while maintaining a sufficent transfer speed for 3D-ToF measurements ((Driewer et al., 2016)) The basic diode structure which was used in this paper was taken from the work of D. Durini, A. Spickermann and A. Suess ((Durini et al., 2010), (Spickermann et al., 2011), (Süss et al., 2013)). In this already enhanced pixel (fig. 1a) the n-well is directly connected to the Floating Diffusion (FD) and the charge is not any longer stored in the well but is accumulated in the FD. The changed accumulation principle is crucial for the presented type of n-well enhancement. Beside the Transfer Gate (TG), there is a second gate for electron accumulation called the Collection Gate (CG), which is set to a constant positive potential. Furthermore a second draining path was implemented (see fig. 1b) to keep the n-well depleted between two accumulation cycles. The electron current can be switched between the signal (FD) and the draining path (DD). The diode also features a lateral doping gradient which provides

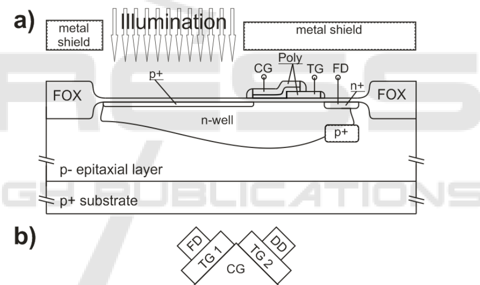

Figure 1: a) Schematic design of the basic diode structure invented by the Fraunhofer IMS in Duisburg and b) top view of the readout and draining path.

Girgenrath L., Hofmann M., KÃijhnhold R. and Vogt H.
Optimization of Transfer Times in Pinned Photodiodes.
DOI: 10.5220/0006239603120316
In *Proceedings of the 5th International Conference on Photonics, Optics and Laser Technology (PHOTOPTICS 2017)*, pages 312-316
ISBN: 978-989-758-223-3
Copyright © 2017 by SCITEPRESS – Science and Technology Publications, Lda. All rights reserved

a built-in electrical field and the connection of the n-well to the FD gives the opportunity to use the reset voltage to implement a stronger electric field to the diode as will be shown.

2 SIMULATION

The potential inside the n-well is pinned to a constant value determined by the p+ top layer and the p substrate and it depends on the doping concentrations. Therefore, the dominating transport mechanism is diffusion which is up to two orders of magnitude slower than the electron transport in an electric field. The pinned photodiode can be interpreted as a simple p-n-p structure and the pinning voltge can be calculated from the built-in potentials of the two p-n-junctions. Thus the pinning voltage depends only on the technology parameters, which are defined by the implantation dose and implantation energy. Therefore, the lateral doping gradient changes the pinning voltage across the length of the diode and provides a built-in electrical field. Since a gradient depends on the length it is applied on, this effect vanishes in bigger sensors. All previous mentioned solutions create an internal field and are not implementable for larger sensors ($>15\,\mu m$). The key to increase the readout speed for large pixels is to introduce a potential difference across the diode bigger than the pinning voltage, which is only possible by bypassing the pinning behaviour. We succeeded to achieve this with a second well implantation to create a designated electron path with a slightly higher doping concentration. The voltage distribution inside the n-well with and without the second implantation is shown in figure 2. The readout voltage is not anymore suppressed by the pinning behaviour. Also the depletion zone is expanded. The implantation is applied at the end of the front end of line so the thermal diffusion is negligible and the doping concentration increases only in a distinct area of the well as an overall higher doping concentration would reduce the width of the depletion zone. However, the transition from the slightly higher doping concentration of the n-well to the doping concentration of the readout node could result in a barrier which slows down the electrons. Figure 3 shows the simulated conduction band energy across the diode for different n-well implantation doses. The barrier-free electron transport requires the conduction band energy to follow a monotonic decreasing function. Figure 4 shows the maximum energy gradient under the CG as well as the maximum voltage drop across the diode for the different implantation doses. Without the second implantation the voltage

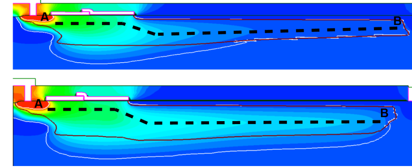

Figure 2: Simulation result of the voltage distribution across the photodiode without the second implantation (top) and with the second implantation (bottom). The electrons travel through the diode on the path from B to A.

drop does not exceed 1 V. The simulations suggest to set the target implantation dose to 3.0e11 cm^{-2}. The increased depletion region increases the quantum efficiency in the IR spectrum but decreases the well capacitance. The pixel performance is not affected by the smaller capacitance as the electrons are stored in the FD. Furthermore, a higher doping concentration reduces the electron drift velocity ((Jacoboni et al., 1977)) in a constant electrical field provided by the pinning voltage. The decrease in mobility is compensated by the 1.7 times stronger voltage gradient which leads to an increased electron speed. Particularly the strong electric field on the well interfaces drives the electrons towards the readout node and the electron velocity at these interfaces with the second implantation is nearly two orders of magnitude higher. The path-time-diagram for one electron based on the velocity calculation (in figure 5) shows that the second implantation can enhance the transfer time of the photodiode doesn't show a strong quadratic dependence anymore. The influence of the strong field at the well interface can be seen as the curve saturates. However, these are the calculations for one electron and the time to ensure complete charge transfer may be a factor of 5-10x longer in any PPD ((Fossum and Hondongwa, 2014)) especially if a barrier is present. It is important for 3D-ToF measurements to reduce the transfer time to a minimum as any remaining charge affects the distance calculation and thus reducing the measurement range. A complete charge transfer after 10 ns is desirable. Therefore, a diode length of $26\,\mu m$ with the second implantation could provide good results.

3 MEASUREMENT

We analyzed five different pixel configurations which differ from each other by their length and implantation scheme. Table 1 shows the main differences between the measured devices. We extended the length of the diode for the second device in order to see the influence as the transfer time rises. The velocity simulations are based on the implantation scheme of pixel C. The higher doping concentration of $3.8e11\,cm^{-2}$

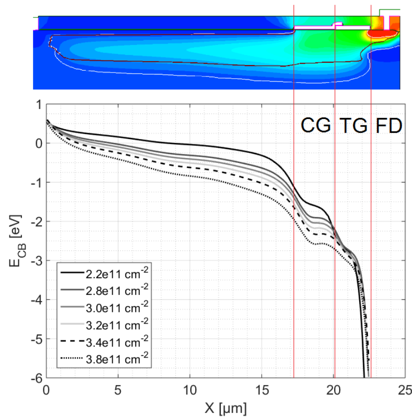

Figure 3: Simulation result of the conduction band energie across the diode for different implantation doses.

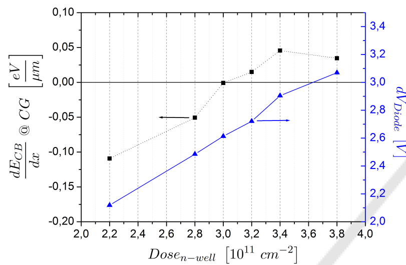

Figure 4: Simulation of the maximum energy gradient under the CG (left, black square) and the maximal voltage drop across the diode (right, blue triangle).

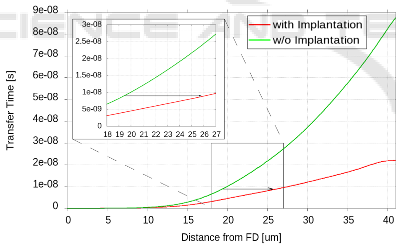

Figure 5: Path-time-diagram for one electron of a simulated 40 μm photodiode along the path from A to B.

for the short reference pixel derive from the optimization of the charge storage. The schematic measurement setup is shown in figure 6. The chip is positioned in-plane with the laser and is illuminated indirectly over two mirrors which redirect the light beam of the laser towards the camera. The mirrors are attached to a moving platform to adjust the distance between the laser and the sensor. We used different distances to change the light itensity on the sensor as the radiation angle of the laser is 10° ($I \propto \frac{1}{r^2}$). The highest possible intensity with a propagation distance of 200 mm is defined as I_0. We measured laser response curves which not only give information about the shutter efficiency but also about the transfer behaviour of the

Table 1: Length and implantation scheme of the measured pixel configurations.

Pixel	Length	n-well Impl.	2nd Impl.
A Ref. Short	19 μm	Phosphorus $3.8e11\ cm^{-2}$	-
B Ref. Low	26 μm	Phosphorus $3.0e11\ cm^{-2}$	-
C Impl. Low	26 μm	Phosphorus $3.0e11\ cm^{-2}$	Phosphorus $1.0e11\ cm^{-2}$
D Ref. High	26 μm	Phosphorus $3.8e11\ cm^{-2}$	-
E Impl. High	26 μm	Phosphorus $3.8e11\ cm^{-2}$	Phosphorus $1.0e11\ cm^{-2}$

electrons. Figure 7 shows the measurement principle to extract the laser response curves. The triggering of the laser and the shutters is performed on-chip and the positions of the pulses refer to this global trigger. The laser pulse is shifted towards the TG1 shutter which is positioned at 75 ns. The laser delay can be adjusted in time steps of 6.25 ns. The laser response is then plotted against the time remaining between TG1 shutter and laser pulse (time before shutter: t_{BFS}) as a function of the propagation delay in respect to the time of flight of the laser pulse. An ideal photodiode with infinite electron speed should not show any signal before the laser and the TG1 shutter overlap. This means that the time the first signal is recorded is equal to the transfer time for a complete charge transfer. All measurements take place in the dark. The background signal of the sensor which is subtracted from the signal is also measured. The TG1 shutter length t_S is set to the lowest value so only electrons with a transfer time between t_{BFS} and $t_{BFS} + t_S$ will contribute to the signal output. The number of accumulation cycles was adjusted to just reach the maximum output for the highest signal level to maintain comparability of the devices and the different t_{BFS}. Therefore, the number of accumulation cycles represent the sensitivity of the sensor. Since the relation between the light intensity and generated electrons is linear, the number of accumulations to fill the readout capacitance should be proportional to the light intensity. We analyze the pixel performance by their charge transfer efficiency. Since the diode is always connected to one of the two draining paths, the charge transfer inefficiency (CTI) is given by the amount of generated electrons which are not effectively drained from the n-well before the TG1 shutter opens and therefore contributing to the FD discharge. The CTI is equal to the voltage drop if the signal reaches the maximum possible output as the accumulations are set to a constant value. For lower signal levels the CTI is calculated in respect to the highest measured signal. An ideal diode with infinite electron speed should show the first signal af-

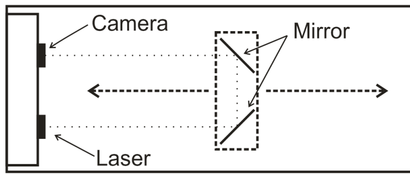

Figure 6: Measurement setup to extract the laser response curves.

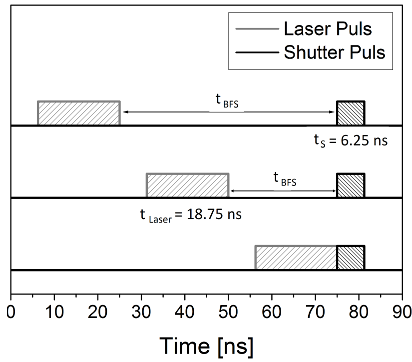

Figure 7: Measurement principle to extract the laser response curves. The signal level is plotted against the time remaining between laser and shutter. The positions refer to the global on-chip trigger.

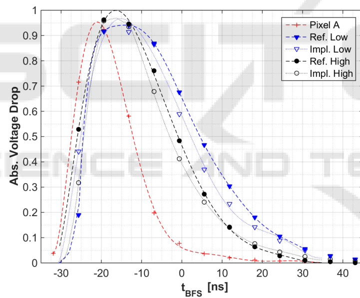

Figure 8: Normalized laser response curves of the five different pixel configurations for I = I_0.

ter the laser and TG-shutter overlaps with no CTI at 0 ns. The corresponding laser response curve of an ideal sensor gives the exact form of the laser pulse. A slower readout speed shifts the peak towards longer transfer times and broadens the measured pulse as the electrons are not drained fast enough from the diode. Therefore, the CTI at 0 ns gives a good idea of the quality of the measured pulse.

4 RESULTS

The measurement results of the different pixel variations are presented in figure 8. The absolute voltage drop is calculated relative to the maximum signal level of the sensor. The increase in diode length from 19 μm (Pixel A) to 26 μm (Ref. High) increases, as expected, the transfer time as well. Directly after the laser puls, 8 % of the charges remain in Pixel A. So the curve represents the laser pulse reasonably well while in the longer version of this pixel (Ref. High) 49 % of the charges remain at 0 ns and the time to reach the same CTI as the short version is up to 20 ns longer. The simulation (fig. 5) shows transfer times of 9 ns for 19 μm and 25 ns for 26 μm which are in good agreement with the measured laser response curves. Reducing only the doping concentration of the n-well results in a stronger influence of the pinning voltage which slows down the readout speed significantly. Therefore, the second implantation enhances the transfer behaviour but not as noticeable as suggested by the simulation. The measurements for lower intensities (fig. 9a and 9b) show an increase in CTI for pixels with a higher n-well doping concentration while the CTI for pixels with lower n-well doping concentration remain stable. As discussed in chapter 2, the increased doping concentration affects the well capacitance and the depletion zone. Also a barrier is formed in the readout path. This effect is observable in the number of accumulation cycles to reach the maximum voltage drop (fig. 10). The relation between the intensity and the number of cycles is not linear for the higher doping concentration. The number of electrons which are generated by incident photons is affected by the depletion zone. As long as there are enough electrons the barrier is not observed in the number of accumulations. Therefore, the influence of the barrier vanishes for higher intensities which provide enough electrons to fill the FD. The second implantation enhances the performance of the pixel but the mismatch between measurement and simulation suggests a barrier in the readout path even for the reduced n-well implantation dose. The barrier is probably formed by bulk effects which are not covered by a 2D simulation. A further enhancement in transfer speed should still be achievable by adjusting the well configuration under the CG.

5 CONCLUSIONS

In this work a new type of n-well enhancement for a pinned photodiode was presented. It has been shown that a local increase in doping concentration of the n-well enhances the transfer speed of a specific type of pinned photodiode. The simulation shows that a 26 μm long photodiode reaches the same performance in terms of transfer speed as a 19 μm long photodiode. Therefore, it is possible to mitigate the quadratic dependence of the transfer time from the diode length.

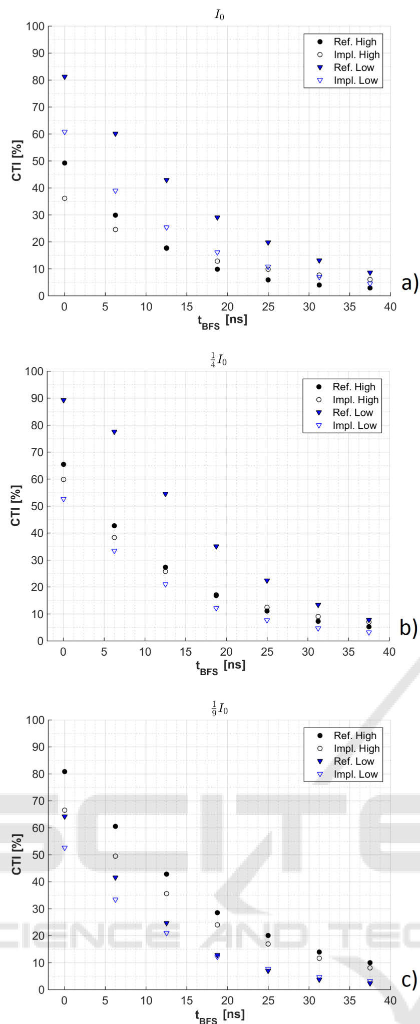

Figure 9: CTI measurements for the longer pixel in relation to the light intensity. a) I = I_0 b) I = 0.25I_0 c) I = 0.11I_0.

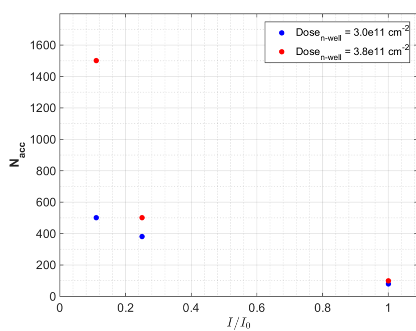

Figure 10: Number of accumulation cycles which are nessesary to reach the maximum voltage drop for different light intensities.

Nevertheless, without prior optimization of the connection of the readout path and the n-well, the transfer behaviour of a 26 μm long PPD was only slightly improved. The readout speed of the full n-well ($t_{BFS} = 0$) was increased by up to 40 % for the same pixel length. For longer transfer times no significant improvement could be achieved due to possible formation of a barrier. However, stable results over a wide intesity range can be achieved if the n-well doping concentration is adjusted in respect to the second implantation. The n-well configuration at the transition between well and readout path remains crucial in terms of transfer speed and will be investigated in the future.

REFERENCES

Driewer, A., Hosticka, B. J., Spickermann, A., and Vogt, H. (2016). Modeling of the charge transfer in a lateral drift field photo detector. *Solid State Electron.*, 126:51–58.

Durini, D., Spickermann, A., Mahdi, R., Brockherde, W., Vogt, H., Grabmaier, A., and Hosticka, B. J. (2010). Lateral drift-field photodiode for low noise, high-speed, large photoactive-area cmos imaging applications. *Nuclear Instruments and Methods in Physics Research Section A: Accelerators, Spectrometers, Detectors and Associated Equipment*, 624:470–475.

Fossum, E. R. and Hondongwa, D. B. (2014). A review of the pinned photodiode for ccd and cmos image sensors. *IEEE J-EDS*, 2:33–43.

Green, M. and Keevers, M. (1995). Optical properties of intrinsic silicon at 300 k. *Progress in Photovoltaics: Research and Applications*, 3:189–192.

Han (2015). A time-of-flight range image sensor with background canceling lock-in pixels based on lateral electric field charge modulation. *IEEE J-EDS*, 3:639–641.

Jacoboni, C., Canali, C., Ottaviani, G., and Quaranta, A. A. (1977). A review of some charge transport properties of silicon. *Solid State Electron.*, 20:77–89.

Spickermann, A., Durini, D., Süss, A., Ulfig, W., Brockherde, W., Hosticka, B. J., Schwope, S., and Grabmaier, A. (2011). Cmos 3d image sensor based on pulse modulated time-of-flight principle and intrinsic lateral drift-field photodiode pixels. *ESSCIRC, 2011 Proceedings of the*, pages 111–114.

Süss, A., Nitta, C., Spickermann, A., Durini, D., Varga, G., Jung, M., Brockherde, W., Hosticka, B. J., Vogt, H., and Schwope, S. (2013). Speed considerations for ldpd based time-of-flight cmos 3d image sensors. *European Solid State Circuits Conference (ESSCIRC)*, pages 299–302.

Tubert, C., Simony, L., Roy, F., Tournier, A., Pinzelli, L., and Magnan, P. (2009). High speed dual port pinned-photodiode for time of flight. *Proc IISW*.

Xu, Y. and Theuwissen, A. J. (2013). Image lag analysis and photodiode shape optimization of 4t cmos pixels. *IISW*, 153.

SCITEPRESS SCIENCE AND TECHNOLOGY PUBLICATIONS